

# Molecular Design Strategy for Simultaneously Strong Luminescence and High Mobility: Multichannel CH- $\pi$ Interaction

Meihui Liu, Yuling Wei, Qi Ou, Peiyi Yu, Guo Wang, Yuai Duan, Hua Geng,\* Qian Peng,\* Zhigang Shuai, and Yi Liao\*



Cite This: *J. Phys. Chem. Lett.* 2021, 12, 938–946



Read Online

ACCESS |



Metrics & More

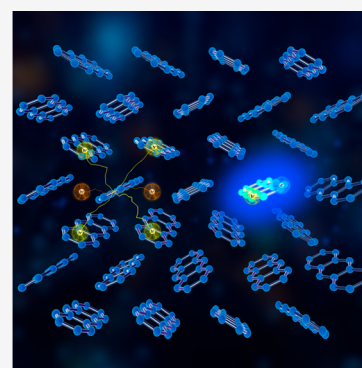


Article Recommendations



Supporting Information

**ABSTRACT:** It is a big challenge to achieve high-performance organic semiconductor materials integrating both high luminescence efficiency and carrier mobility, because they are commonly regarded as a pair of contradiction. Here, combining a tight-binding model and density functional theory/time-dependent density functional theory, we propose a theoretical protocol to characterize the luminescence efficiency via an excitonic effective mass and charge transport ability via charge effective mass at the same level. Applying this protocol to a series of organic semiconductor materials, we find that the multichannel CH- $\pi$  interaction can induce a heavy excitonic effective mass and light charge effective mass, which effectively balance the light-emitting efficiency and carrier mobility. Thus, a practical molecular design strategy is figured out to exploit novel organic semiconductor materials with strong luminescence and fast carrier transport simultaneously.



Molecular semiconductors for logic operations offer plenty of opportunities in materials chemistry.<sup>1</sup> Organic light-emitting transistors and organic electrically pumped lasers have attracted tremendous interests in recent years.<sup>2–11</sup> These two kinds of devices require organic semiconductors with a strong solid-state luminescence and high charge mobility. For these two types of devices, according to Langevin's model, the nonradiative carrier recombination rate is expressed as  $k_{nr} = \frac{q}{\epsilon}(\mu_e + \mu_h)$ , where  $q$  is the carrier charge, and  $\mu_{e(h)}$  is the electron (hole) mobility. Therefore, high mobility would in general lead to luminescence quenching.<sup>12,13</sup> Low carrier mobilities, however, could cause injected charge absorption loss and electrical contact loss, eventually increasing the pump energy required to reach the lasing threshold.<sup>14,15</sup> For organic materials, a closely stacking  $\pi$ - $\pi$  conformation has always been regarded as a prerequisite for achieving high mobility materials. Thus, diverse substitutions have been introduced to modulate intermolecular stacking and facilitate charge transport.<sup>16–18</sup> Nevertheless, a strong  $\pi$ - $\pi$  interaction usually quenches the luminescence owing to the formation of H-aggregation, excimer, or exciplex.<sup>19</sup>

The typical charge transport materials, as seen in (Scheme 1), with high mobility, such as rubrene,<sup>20–24</sup> thienoacene derivatives (C12-BTBT),<sup>25</sup> and  $\alpha$ -linked oligothiophene ( $\alpha$ -4T),<sup>26,27</sup> all have very weak fluorescence, as seen in Figure 1. There are some materials,<sup>28–31</sup> such as DTAnt<sup>32</sup> and DPVAnt,<sup>33</sup> which exhibit good charge transport properties but do not emit light at all. For systems with moderate mobility, such as BSPAnt, BOPAnt, BEPAnt,<sup>34</sup> and 2A,<sup>35</sup> their solid-state luminescence properties have not been reported at

present, although their fluorescence is not weak in solution. Recently, several anthracene derivatives, such as 2,6-diphenylanthracene (DPA)<sup>36</sup> and dNaAnt,<sup>37</sup> have been excitedly found to exhibit a high solid-phase luminescent efficiency and charge mobility simultaneously, offering great opportunities to become the excellent organic semiconductors integrating excellent charge transport with a high-efficiency solid emission.<sup>38–40</sup>

Aggregation-caused quenching (ACQ) luminescence has been generally recognized to be a prevailing characteristic of conventional aromatic  $\pi$ -conjugated luminophores,<sup>41–43</sup> which prevents them from achieving a high-efficiency luminescence in a solid phase or aggregation phase and limits the applications of those luminophores in practice.<sup>44–48</sup> To solve the knotty problem of ACQ, lots of strategies have been proposed to modulate intermolecular packing, for instance, introducing bulky units to attenuate intermolecular  $\pi$ - $\pi$  interactions,<sup>49</sup> tuning the molecular stacking orientation in a cross mode to generate X-aggregation,<sup>50</sup> or enlarging intermolecular displacement to evolve into J-aggregation stacking modes.<sup>51</sup> Note that, in these strategies, the prerequisite is to maintain the  $\pi$ - $\pi$  interaction as much as possible, which is commonly considered to be indispensable for good carrier transport. In practice, there

Received: November 20, 2020

Accepted: January 11, 2021

Published: January 13, 2021



Scheme 1. Reported Molecular Structures of Typical Semiconductor Materials

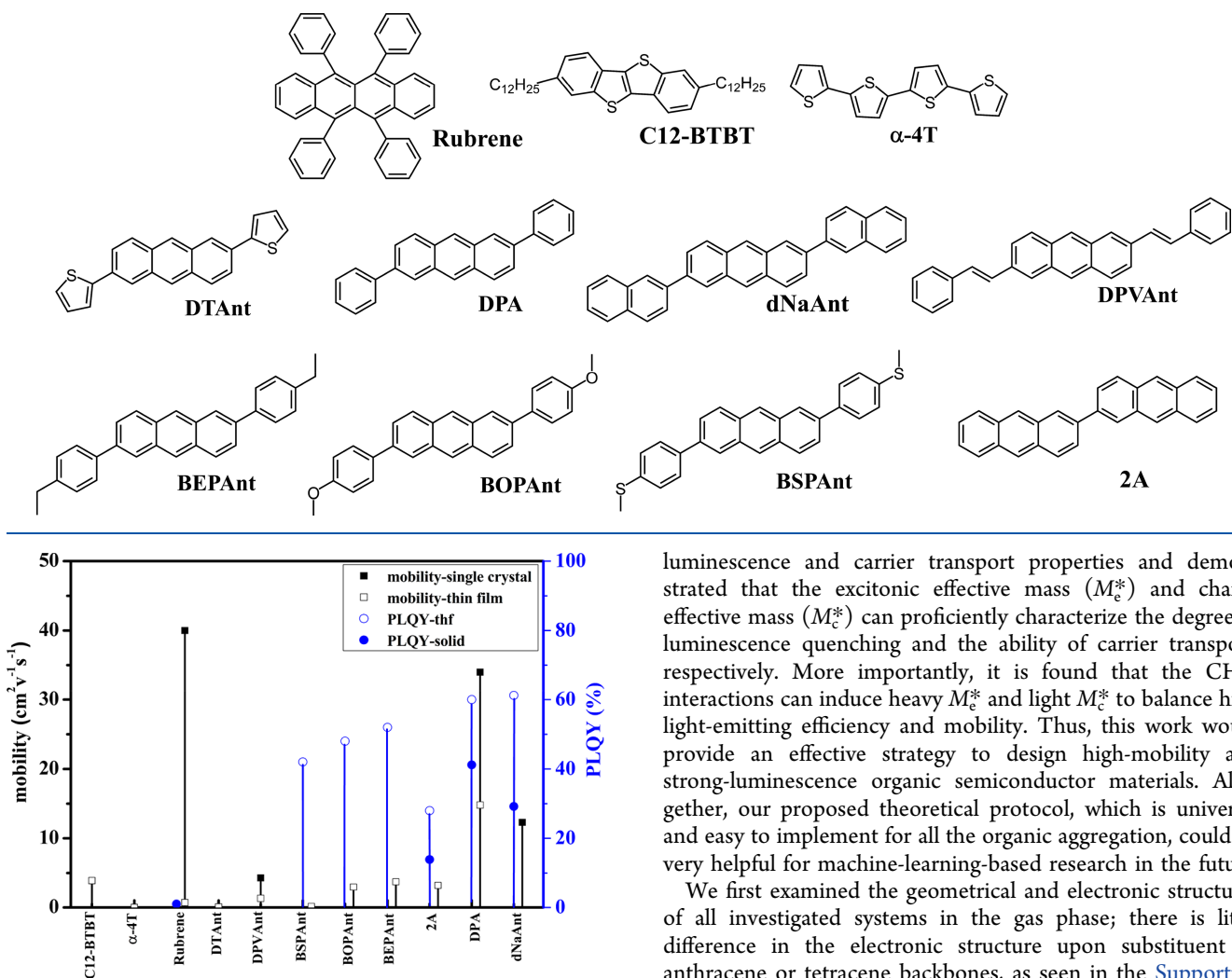


**Figure 1.** Single-crystal and film charge mobility and the photoluminescence quantum yield (PLQY) in solution and solid reported in the literature.

are various types of intermolecular interactions, such as cation- $\pi$ , anion- $\pi^+$ ,  $\pi_{\text{cation}}-\pi$ , hydrogen bonding, halogen bonding,  $\pi$ -halogen bonding,  $\pi-\pi$ , and CH- $\pi$  interactions in organic aggregates.<sup>52,53</sup> It is still not clear how those types of interactions affect the luminescent and carrier transport properties. Intuitively, the charge transport is driven by the electronic coupling between two neighboring molecules, which is approximately characterized by their overlap of highest occupied molecular orbital (HOMO) for hole transport or lowest unoccupied molecular orbital (LUMO) for electron transport,<sup>54</sup> while the luminescence is affected by the excitonic coupling, which is closely related to the overlap of HOMO and LUMO between two adjacent molecules.<sup>55–57</sup> These two parameters may perform differently in different scenarios. Therefore, it is necessary to investigate the explicit dependency relationship of the luminescence and charge transport on the intermolecular interactions and come up with a uniform descriptor to characterize the luminescence property and charge transport ability at the same theoretical level.

With that in mind, we proposed a theoretical protocol to disclose the effect of the intermolecular interaction on

luminescence and carrier transport properties and demonstrated that the excitonic effective mass ( $M_c^*$ ) and charge effective mass ( $M_e^*$ ) can proficiently characterize the degree of luminescence quenching and the ability of carrier transport, respectively. More importantly, it is found that the CH- $\pi$  interactions can induce heavy  $M_c^*$  and light  $M_e^*$  to balance high light-emitting efficiency and mobility. Thus, this work would provide an effective strategy to design high-mobility and strong-luminescence organic semiconductor materials. Altogether, our proposed theoretical protocol, which is universal and easy to implement for all the organic aggregation, could be very helpful for machine-learning-based research in the future.

We first examined the geometrical and electronic structures of all investigated systems in the gas phase; there is little difference in the electronic structure upon substituent to anthracene or tetracene backbones, as seen in the [Supporting Information](#). And thus, further theoretical investigations are performed to elucidate the diverse charge transport and luminescence properties of these molecules in the solid phase. The experimental lattice parameters of these systems are listed in [Table S4](#), and the selected ones are displayed in [Figure 2](#). It is easily seen that two kinds of interactions are dominant for all the systems, that is,  $\pi-\pi$  interaction and XH- $\pi$  ( $X = C, S$ ) interaction, as indicated in [Scheme 2](#) and [Figure 2](#). The  $\pi-\pi$  interaction corresponds to a face-to-face parallel-displaced conformation, and the CH- $\pi$  one refers to an edge-to-face stacking conformation, which is also called T-shaped  $\pi-\pi$ . The central molecule has four CH- $\pi$  neighboring molecules, while there are two face-to-face  $\pi-\pi$  stacking neighboring molecules, and thus, multichannel charge and exciton transfer pathways can be achieved through an edge-to-face (CH- $\pi$ ) stacking direction. The CH- $\pi$  interactions in anthracene derivatives are very strong with the short centroid distances  $d_{\text{XH}-\pi}$  ranging from 2.627 to 3.081 Å and small angles  $\beta < 12.8^\circ$ , while the  $\pi-\pi$  interactions are weak owing to a large slip between  $\pi$ -conjugated planes. In particular, DPA has the largest slip along the long axis and the smallest distance (2.294 Å) between the two  $\pi-\pi$  interaction surfaces, which considerably decrease the intermolecular  $\pi-\pi$  interaction. The  $\pi-\pi$  interaction is expected to be dominant in rubrene because of its face-to-face molecular packing of  $\pi$ -conjugated planes. To quantitatively measure the intermolecular interactions, we calculated

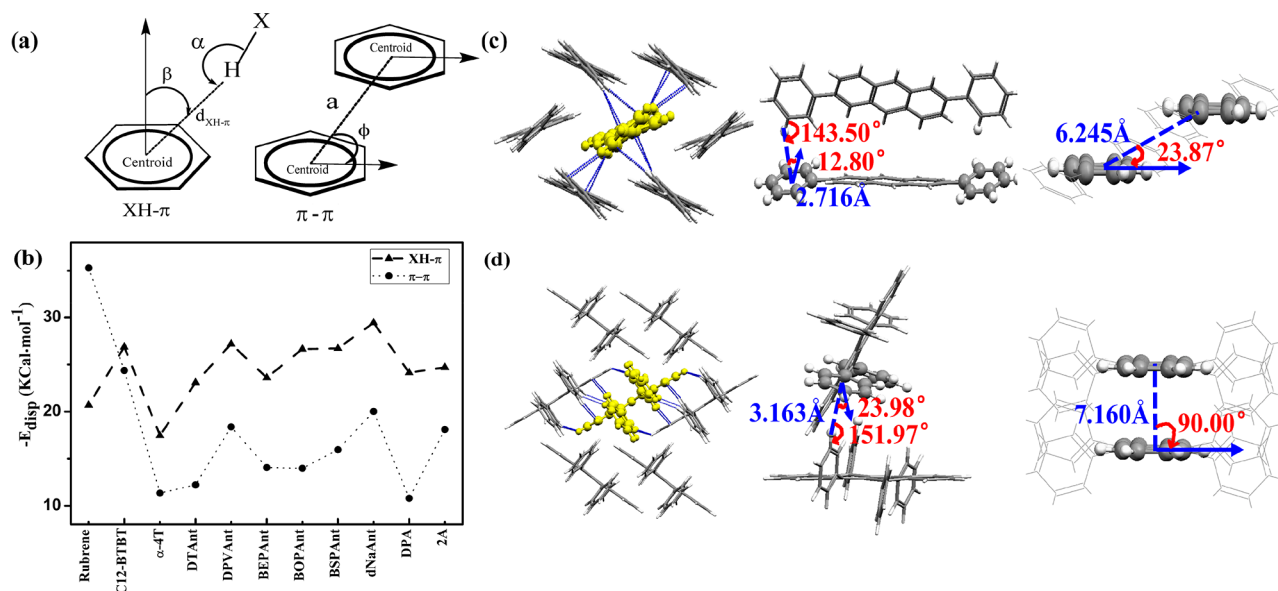
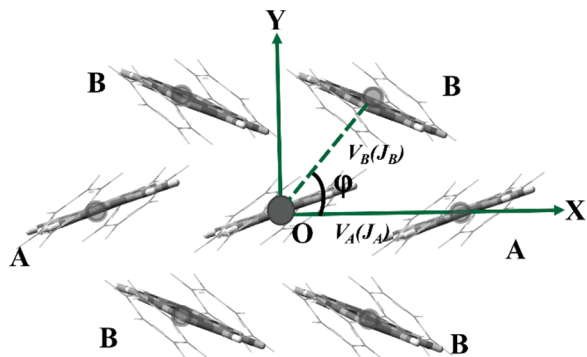


**Figure 2.** (a) The two kinds of interactions, XH- $\pi$  and  $\pi$ - $\pi$ . (b) The dispersion energies along XH- $\pi$  and  $\pi$ - $\pi$  directions for all investigated systems. Close contact intermolecular interactions of DPA (c) and rubrene (d) along different stacking directions, are shown by the dotted lines.

### Scheme 2. 2D Lattice Model for DPA in Herringbone Plane



the dispersion energies  $E_{\text{disp}}$  and total interaction energies  $E_{\text{tot}}$  by using an extended version of the symmetry-adapted perturbation theory (SAPT) and many-body dispersion (MBD) method (XSAPT+MBD)<sup>58</sup> in the Q-Chem package<sup>59</sup> and plotted the results in Figure 2b (the detailed energy decompositions are listed in Table S5). As expected, the CH- $\pi$  interaction is stronger than that of the  $\pi$ - $\pi$  interaction in anthracene derivatives. Herein, DPA reveals the weakest  $\pi$ - $\pi$  interaction among all the investigated systems. However, the  $\pi$ - $\pi$  interaction is dominant in rubrene due to a stronger dispersion energy. Both CH- $\pi$  and  $\pi$ - $\pi$  interactions are important in C12-BTBT. The different interactions could have different effects on the luminescence and charge transport properties.

As expected, owing to the different intermolecular interactions, the excitonic couplings ( $J$ ) and electronic couplings ( $V$ ) vary significantly for the investigated systems (see Table S6). For excitonic coupling, the values along the CH- $\pi$  direction ( $J_B$ ) are mostly larger than those along the  $\pi$ - $\pi$  direction ( $J_A$ ), which is consistent with a stronger CH- $\pi$  interaction than a  $\pi$ - $\pi$  interaction in the systems as discussed above. It is however found that there is not a monotonic correlation between the strength of excitonic coupling and the degree of fluorescence quenching. The  $\alpha$ -4T has the largest

excitonic couplings of  $J_A = 89.92$  meV and  $J_B = 95.82$  meV, explaining well its weak fluorescence in the crystalline phase.<sup>60</sup> Nevertheless, the small excitonic couplings of  $J_A = 20.93$  meV and  $J_B = 19.36$  meV of rubrene cannot rationalize its extremely serious fluorescence quenching. For electronic coupling, the values in the  $\pi$ - $\pi$  direction ( $V_A$ ) are much larger than those in the CH- $\pi$  direction ( $V_B$ ) for rubrene and C12-BTBT, while  $V_A$  are smaller than  $V_B$  for the other systems, which is also in line with the dispersion energy shown in Figure 2. Although there is a relatively positive correlation between the electronic coupling and the mobility, the effect of a multichannel CH- $\pi$  charge transfer effect on charge transport has not been accounted for.

To shed light on the different dependence of the excitonic and electronic coupling on the molecular packing conformation, we further scan the two couplings along the  $\pi$ - $\pi$  direction and CH- $\pi$  direction in DPA. Starting from a dimer taken from an X-ray diffraction (XRD) crystal along  $\pi$ - $\pi$  direction, we displace a monomer in the central anthracene plane as displayed in Figure 3a to calculate the corresponding excitonic and electronic couplings in Figure 3c,d, respectively; it is found that (i) the two kinds of couplings perform differently, as analyzed above; (ii) the excitonic coupling varies slowly, while the electronic coupling changes sharply with the displacement, which indicates that the electronic coupling is much more sensitive to a  $\pi$ - $\pi$  interaction than the excitonic coupling; (iii) the two kinds of interactions are very weak for DPA with  $J < 20$  meV and  $V < 30$  meV; thus, the  $\pi$ - $\pi$  direction does not contribute much to the luminescence and mobility in herringbone stacking due to the large lateral displacement. The CH- $\pi$  interaction exhibits asynchronous changes in excitonic coupling and electronic coupling. Keeping the intermolecular centroid distance unchanged, we rotate a monomer along the long axis to change the herringbone angle from  $0^\circ$  to  $60^\circ$  (see Figure 3b), in which the transition dipole moments of two molecules are still closely parallel, which results in an almost unchanged excitonic coupling, as seen in Figure 3e, while the electronic coupling changes dramatically, because it is highly susceptible to the relative orientations and

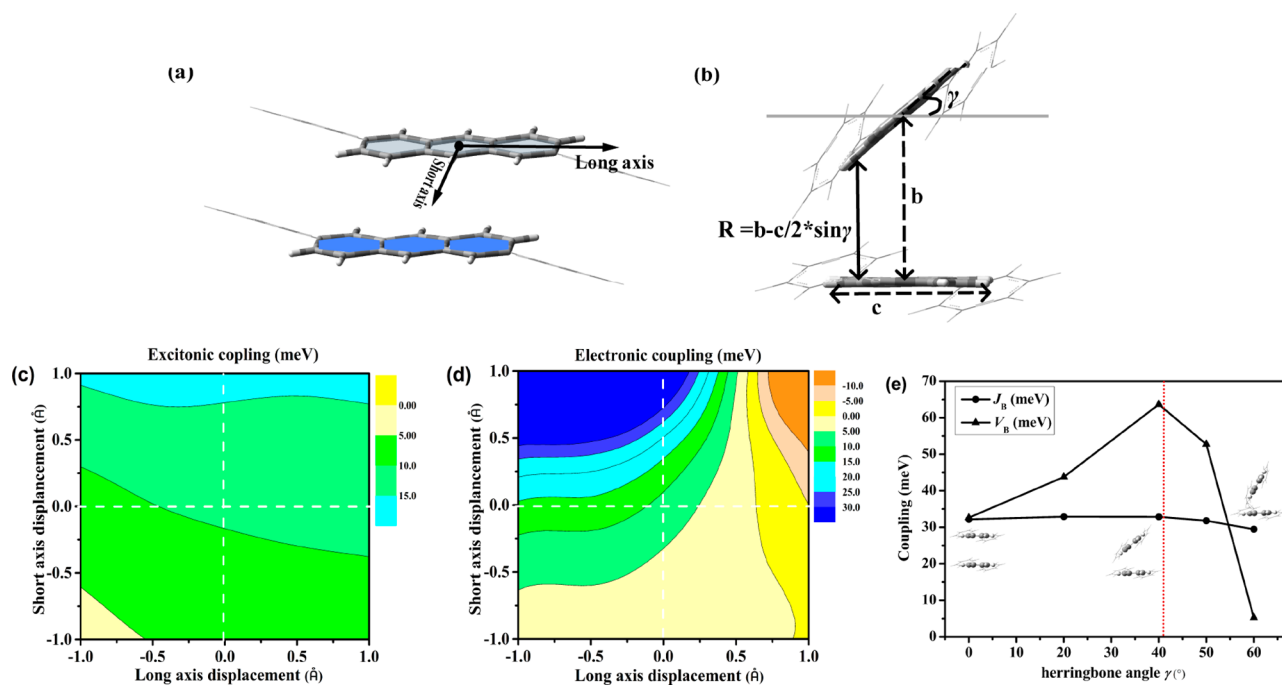


**Figure 3.** (a) The intermolecular displacement in the central anthracene plane. (b) The model of herringbone angle  $\gamma$  in CH- $\pi$  direction. The evolution of excitonic couplings (c) and electronic couplings (d) as a function of displacement in the central anthracene plane. (e) Evolution of the electronic couplings and excitonic couplings as a function of the herringbone angle  $\gamma$ . The red dotted line indicates the herringbone angle ( $\gamma = 41.52^\circ$ ) in the actual DPA crystal.

packing characters of the molecules as displayed. When the intermolecular herringbone angle is  $40^\circ$ , the electronic coupling reaches the maximum, as labeled by the red line. Excitingly, the smallest excitonic coupling and largest electronic coupling are almost achieved simultaneously at the herringbone angle  $\gamma = 41.52^\circ$  for a DPA crystal, which suggests that strong luminescence and high charge transport can be effectively balanced. Therefore, the modulation of CH- $\pi$  interaction could provide a design strategy for a strong luminescence and high charge mobility simultaneously.

It is difficult to clarify the solid-state luminescence and charge transport only from a dimer configuration; the exciton band dispersion in organic crystals should be considered as well. And thus, we combined a Tight Binding (TB) model and time-dependent density functional theory (TDDFT) parameters; the excitonic energy band structures can be generated. To discuss the electronic and excitonic band structures at the same level, we similarly combine density functional theory (DFT) and a TB approximation to calculate electronic band structures, which can give consistent results with those obtained by a periodic first-principle calculation, as indicated in Figure S2.

All investigated systems are aligned closely in the herringbone plane, while a large intermolecular distance is acquired between neighboring molecules in the perpendicular direction. Thus, the intermolecular coupling in the perpendicular direction can be neglected.<sup>61</sup> Taking DPA as an example, we present its projection along a molecular long axis in Scheme 2, in which one molecule is surrounded by six nearest-neighbor molecules. Molecules along the  $\pi$ - $\pi$  stacking direction are labeled as A, and those along the CH- $\pi$  direction are labeled as B. A two-dimension (2D) lattice model is established with two equivalent A molecules and four equivalent B molecules as shown in Scheme 2. On the basis of the TB model, we consider

six nearest neighbors, and the band dispersion of investigated system can be expressed as

$$E(k) = E_0 + 2J_A \cos(a \cdot k_x) + 4J_B \cos(b \cos \varphi \cdot k_x) \cdot \cos(b \sin \varphi \cdot k_y) \quad (1)$$

Here,  $E_0$  corresponds to the excited energy of an isolated molecule.  $a$  ( $b$ ) is the intermolecular centroid distance between the central and neighboring molecule A (B).  $\varphi$  represents the angle between OA and OB.  $J_A$  ( $J_B$ ) is the excitonic coupling along OA (OB). The effective mass at the excitonic band minimum (X and Y) is derived as

$$m_{k_x}^* = \frac{\hbar^2}{-2J_A \cdot a^2 + 4J_B (b \cos \varphi)^2}$$

$$m_{k_y}^* = \frac{\hbar^2}{4J_B (b \sin \varphi)^2} \quad (2)$$

From Equation 2, it is obvious that the excitonic effective mass is determined by not only the excitonic coupling but also the stacking structure parameters, including the intermolecular centroid distance ( $a$ ) and the stacking angle ( $\varphi$ ). Furthermore, the multichannel feature is also conscientiously characterized through the number of nearest molecules around one central molecule in the equation. Since all investigated systems belong to H-like aggregates with  $J > 0$  (see Table S6 in the Supporting Information),<sup>55</sup> the excitonic coupling always quenches luminescence. Hence, a strong luminescence requires a small excitonic coupling, which corresponds to large effective mass according to Equation (2). Under the Frenkel exciton model, the excitonic coupling between two molecules can be evaluated by  $J_{m,n}^e = \langle \Phi_m^e \Phi_n^s | H | \Phi_m^s \Phi_n^e \rangle$ , which can be simplified as solving

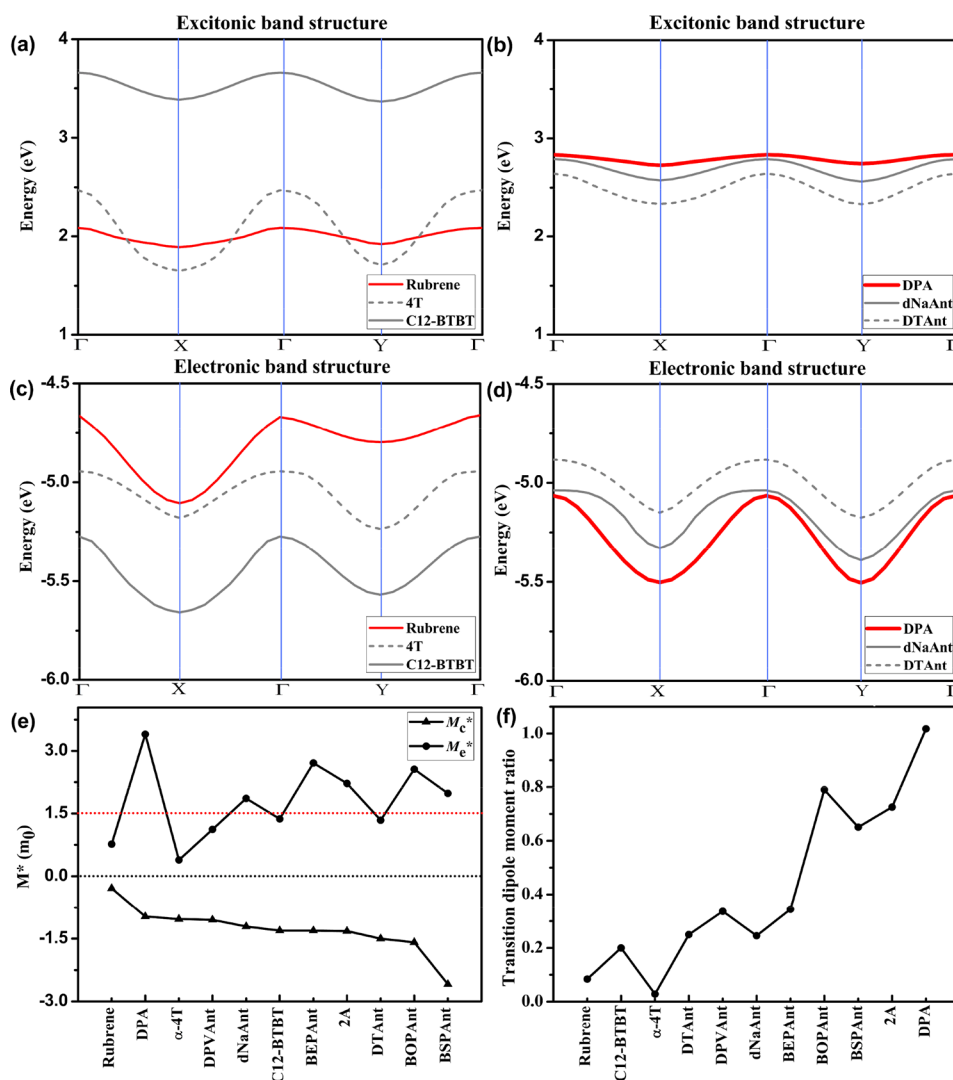


**Figure 4.** Excitonic band structure (a, b) and electronic band structure (c, d) based on a DFT/TDFT parametrized tight-binding model. The reciprocal coordinates of high-symmetry points are  $\Gamma = (0, 0, 0)$ ,  $X = (0.5, 0, 0)$ , and  $Y = (0, 0.5, 0)$ . (e) The charge effective mass ( $M_e^*$ ) and excitonic effective mass ( $M_e^*$ ) and (f) the transition dipole moment ratio ( $\mu_{dimer}/\mu_{monomer}$ ) in the dominant direction.

a coulomb integral and exchange integral between molecular orbitals according to Wick's theorem.<sup>62</sup>

Similarly, the electronic band structure can be also obtained by Equation 1 in which  $E_0$  alternatively points to the charge site energy of an isolated molecule, and the  $J_A$  ( $J_B$ ) is replaced by the electronic coupling  $V_A$  ( $V_B$ ), as displayed in Scheme 2. In the case of hole transport, the effective mass at valence band maximum ( $\Gamma$  point) recasts:

$$m_{k_x}^* = \frac{-\hbar^2}{2V_A \cdot a^2 + 4V_B(b \cos \varphi)^2}$$

$$m_{k_y}^* = \frac{-\hbar^2}{4V_B(b \sin \varphi)^2} \quad (3)$$

Within the band regime, the carrier mobility is inversely proportional to  $lm^*$ .<sup>63,64</sup> In other words, the lighter the effective mass is, the higher the carrier mobility will be. The electronic coupling can be calculated by site energy correction method and mainly controlled by the overlap of HOMO or LUMO between two neighboring molecules, which is very sensitive to the relative displacement and orientation between

two molecules.<sup>65,66</sup> When Equation 2 and Equation 3 are compared, it is easily known that the excitonic and electronic effective masses exhibit a different dependence on the molecular packing parameters.

According to Equation 1, the excitonic and electronic band structures are obtained to analyze the exciton and charge transfer properties at the same level, as shown in Figure 4a–d and Figure S3. In the case of rubrene, it can be seen that the excitonic band exhibits very small dispersion with bandwidths of 0.18 and 0.15 eV along the  $\Gamma X$  and  $\Gamma Y$  directions, respectively, while its electronic band indicates a significant dispersion with bandwidth (0.44 eV) in the  $\Gamma X$  direction and a nearly flat electronic band in the  $\Gamma Y$  direction.

For C12-BTBT, there is a similar excitonic band dispersion with equal bandwidth (0.29 eV) along the  $\Gamma X$  and  $\Gamma Y$  directions. The electronic band reveals larger band dispersion with bandwidth (0.38 eV) along the  $\Gamma X$  direction. For the  $\alpha$ -4T system, there are much larger excitonic band dispersions with bandwidths of 0.84 and 0.77 eV along the  $\Gamma X$  and  $\Gamma Y$  directions, respectively, while there is a small electronic band dispersion with 0.29 eV both in  $\Gamma X$  and  $\Gamma Y$  directions. The anthracene derivatives, owing to a multichannel  $CH-\pi$

interaction, exhibit a similar band dispersion in both GX and GY directions. From DTAnt and dNaAnt to DPA, the excitonic band dispersion gradually gets smaller, while the electronic band becomes larger, which is consistent with first-principle electronic band structure results, as shown in Figure S2. Other anthracene systems reveal similar properties, as seen in Figure S3. Overall, the excitonic band shows different variation trends with electronic band structure, because they originate from a different dependence relationship on an intermolecular herringbone angle, as mentioned in Figure 4e. Among them, DPA exhibits the largest electronic band dispersion, which facilitates the charge transfer, and the smallest excitonic band dispersion, which means the smallest excitation splitting energy, generating the least fluorescence quenching as observed in experiment.<sup>36</sup>

On the basis of the band structures, we further calculate the excitonic effective mass ( $M_e^*$ ) and charge effective mass ( $M_c^*$ ). As shown in Figure 4e, we find that rubrene presents a relatively light excitonic effective mass ( $M_e^*$ ) (0.77  $m_0$ ) in the GY direction due to the large intermolecular centroid distance ( $b = 7.93 \text{ \AA}$ ), which could significantly quench the luminescence as seen in an experiment.<sup>20</sup> Similarly, it also processes remarkably light ( $-0.29 m_0$ ) along the GX ( $\pi-\pi$ ) direction owing to a large intermolecular centroid distance and a significantly strong electronic coupling  $V_A$  (93.9 meV), which results in the high-speed hole transport, as experimental results show in Figure 1. C12-BTBT and  $\alpha$ -4T have very light  $M_e^*$  (1.37  $m_0$ , 0.39  $m_0$ ) and  $M_c^*$  ( $-1.26 m_0$ ,  $-1.03 m_0$ ) values, indicating a strong luminescence quenching and rapid hole transport, which is consistent with weak luminescence and high charge mobility as seen in Figure 1. From DTAnt and dNaAnt to DPA, the  $M_e^*$  turns larger and larger, while the  $M_c^*$  becomes smaller and smaller. In particular, DPA exhibits the heaviest  $M_e^*$  (3.40  $m_0$ , 4.83  $m_0$ ) and the smallest  $M_c^*$  ( $-1.01 m_0$ ,  $-0.97 m_0$ ) in both GX and GY directions, which indicates that the strong luminescence and charge transport are balanced in DPA. The positive correlation between the effective mass and the luminescence and transport properties is also found in other anthracene derivatives (see Figure S3 and Table S6). Therefore, it is safe to say that the excitonic effective mass  $M_e^*$  and charge effective mass  $M_c^*$  are two good descriptors to characterize the degree of luminescence quenching and the ability of charge transport at the same theoretical level.

In addition, we discuss the aggregation effect on a radiative process through the transition dipole moment variations from the monomer to dimer, as seen in Figure 4f. The larger excitonic effective mass means the less aggregation-quenching effect; that is, the transition dipole moment ratio of monomer to dimer  $\mu_{\text{dimer}}/\mu_{\text{monomer}}$  is closer to 1. Among the systems in Figure 4f, the  $\mu_{\text{dimer}}/\mu_{\text{monomer}}$  of DPA is close to 1, while those of rubrene, C12-BTBT, and  $\alpha$ -4T are largely reduced to 0, which fully supports the conclusion drawn from the effective mass as discussed above. Therefore, a positive correlation is further confirmed between the excitonic effective mass ( $M_e^*$ ) and the degree of luminescence quenching through a nonradiative energy transfer. This also suggests that the energy transfer is an important nonradiative processes in organic semiconductor aggregates systems, although there are other nonradiative decay processes, such as singlet fission and charge transfer and so on. Note that we just consider long-range Coulomb coupling, CT-mediated superexchange excitonic coupling,<sup>67</sup> and the coupling between the CT state and Frenkel exciton have not been accounted for;<sup>68</sup> we will

systematically investigate the effect of the CT state on the promising organic semiconductor materials in the future.

In summary, we propose a theoretical protocol to characterize the luminescence property by an excitonic effective mass and charge transport capability by charge effective mass at the same theoretical level. Applying this protocol to a series of organic semiconductor materials, we find that an excitonic and electronic band structure and a corresponding effective mass present different variation trends. In the case of anthracene derivatives, a  $\pi-\pi$  interaction does not contribute much to the luminescence and mobility in herringbone stacking due to the lateral displacement. For a CH- $\pi$  interaction, we can adjust the herringbone angle through substitution so as to obtain the largest possible electronic coupling, while keeping small excitonic coupling unchanged. Thus, multichannel CH- $\pi$  interactions can induce a heavy excitonic effective mass ( $M_e^*$ ) and a light charge effective mass ( $M_c^*$ ), which can balance a high light-emitting efficiency and mobility. Altogether, we have proposed a molecular design strategy to balance the contradictory charge transport and luminescent properties through a substitution-monitored intermolecular multichannel CH- $\pi$  interaction. This strategy allows us to modulate the stacking structure in the CH- $\pi$  direction to ameliorate "aggregation (or concentration) quenching" in solid-phase conjugated materials. This work could provide an effective strategy to design high-mobility and strong-luminescence organic semiconductor materials. Moreover, our theoretical protocol is universal and easy to implement for all the organic aggregation, which could be very helpful for the machine-learning-based molecular screening in the future.

## ■ ASSOCIATED CONTENT

### Supporting Information

The Supporting Information is available free of charge at <https://pubs.acs.org/doi/10.1021/acs.jpcllett.0c03453>.

Computational details for electronic structure; optimized and experimental XRD geometric structures; the frontier molecular orbitals and transition dipole moment; energy level of  $S_1$  and  $T_1$ ; intermolecular interaction parameters; XSAPT+MBD energy decomposition; electronic couplings and excitonic couplings; hole effective mass and excitonic effective mass; electronic band structure (PDF)

## ■ AUTHOR INFORMATION

### Corresponding Authors

Hua Geng – Department of Chemistry, Beijing Advanced Innovation Center for Imaging Theory and Technology Capital Normal University, Beijing 100048, China; [orcid.org/0000-0001-6485-1339](https://orcid.org/0000-0001-6485-1339); Email: [hgeng@cnu.edu.cn](mailto:hgeng@cnu.edu.cn)

Qian Peng – School of Chemical Sciences, University of Chinese Academy of Sciences, Beijing 100049, China; [orcid.org/0000-0001-8975-8413](https://orcid.org/0000-0001-8975-8413); Email: [qpeng@iccas.ac.cn](mailto:qpeng@iccas.ac.cn)

Yi Liao – Department of Chemistry, Beijing Advanced Innovation Center for Imaging Theory and Technology Capital Normal University, Beijing 100048, China; Email: [yliao@cnu.edu.cn](mailto:yliao@cnu.edu.cn)

## Authors

- Meihui Liu – Department of Chemistry, Beijing Advanced Innovation Center for Imaging Theory and Technology Capital Normal University, Beijing 100048, China
- Yuling Wei – Department of Chemistry, Beijing Advanced Innovation Center for Imaging Theory and Technology Capital Normal University, Beijing 100048, China
- Qi Ou – Department of Chemistry, Tsinghua University, Beijing 100083, China; [orcid.org/0000-0002-6400-7522](https://orcid.org/0000-0002-6400-7522)
- Peiyi Yu – Department of Chemistry, Beijing Advanced Innovation Center for Imaging Theory and Technology Capital Normal University, Beijing 100048, China
- Guo Wang – Department of Chemistry, Beijing Advanced Innovation Center for Imaging Theory and Technology Capital Normal University, Beijing 100048, China
- Yuai Duan – Department of Chemistry, Beijing Advanced Innovation Center for Imaging Theory and Technology Capital Normal University, Beijing 100048, China
- Zhigang Shuai – Department of Chemistry, Tsinghua University, Beijing 100083, China; [orcid.org/0000-0003-3867-2331](https://orcid.org/0000-0003-3867-2331)

Complete contact information is available at:

<https://pubs.acs.org/10.1021/acs.jpcllett.0c03453>

## Notes

The authors declare no competing financial interest.

## ACKNOWLEDGMENTS

This work is supported by National Key R&D Program of China (2017YFA0204700 and 2017YFA0204502) and the National Natural Science Foundation of China (21673247 and 21973099), Beijing Municipal Natural Science Foundation (2192013 and 2182012) and Capacity Building for Sci-Tech Innovation-Fundamental Scientific Research Funds (19530012018 and 19530011018), and the Strategic Priority Research Program of the Chinese Academy of Sciences (XDB12020200).

## REFERENCES

- (1) Schweicher, G.; Garbay, G.; Jouclas, R.; Vibert, F.; Devaux, F.; Geerts, Y. H. Molecular Semiconductors for Logic Operations: Dead-End or Bright Future? *Adv. Mater.* **2020**, *32*, No. e1905909.
- (2) Liu, C.; Liu, X.; Lai, W.; Huang, W. Organic Light-Emitting Field-Effect Transistors: Device Geometries and Fabrication Techniques. *Adv. Mater.* **2018**, *30*, No. 1802466.
- (3) Choi, S.; Kang, C. M.; Byun, C. W.; Cho, H.; Kwon, B. H.; Han, J. H.; Yang, J. H.; Shin, J. W.; Hwang, C. S.; Cho, N. S.; et al. Thin-Film Transistor-Driven Vertically Stacked Full-Color Organic Light-Emitting Diodes for High-Resolution Active-Matrix Displays. *Nat. Commun.* **2020**, *11*, 2732.
- (4) Ciccoira, F.; Santato, C. Organic Light Emitting Field Effect Transistors: Advances and Perspectives. *Adv. Funct. Mater.* **2007**, *17*, 3421–3434.
- (5) Muccini, M. A Bright Future for Organic Field-Effect Transistors. *Nat. Mater.* **2006**, *5*, 605–613.
- (6) Ou, Q.; Peng, Q.; Shuai, Z. Computational Screen-Out Strategy for Electrically Pumped Organic Laser Materials. *Nat. Commun.* **2020**, *11*, 4485.
- (7) Lin, Y. H.; Li, W.; Faber, H.; Seithkan, A.; Hastas, N. A.; Khim, D.; Zhang, Q.; Zhang, X.; Pliatsikas, N.; Tsetseris, L.; et al. Hybrid Organic-Metal Oxide Multilayer Channel Transistors with High Operational Stability. *Nat. Electron.* **2019**, *2*, 587–595.
- (8) Hou, L.; Zhang, X.; Cotella, G. F.; Carnicella, G.; Herder, M.; Schmidt, B. M.; Patzel, M.; Hecht, S.; Cacialli, F.; Samori, P. Optically Switchable Organic Light-Emitting Transistors. *Nat. Nanotechnol.* **2019**, *14*, 347–353.
- (9) Zaumseil, J.; Friend, R. H.; Sirringhaus, H. Spatial Control of The Recombination Zone in An Ambipolar Light-Emitting Organic Transistor. *Nat. Mater.* **2006**, *5*, 69–74.
- (10) Capelli, R.; Toffanin, S.; Generali, G.; Usta, H.; Facchetti, A.; Muccini, M. Organic Light-Emitting Transistors with an Efficiency that Outperforms The Equivalent light-Emitting Diodes. *Nat. Mater.* **2010**, *9*, 496–503.
- (11) Wakayama, Y.; Hayakawa, R.; Seo, H. S. Recent Progress in Photoactive Organic Field-Effect Transistors. *Sci. Technol. Adv. Mater.* **2014**, *15*, 024202.
- (12) Langevin, P. The Recombination and Mobilities of Ions in Gases. *Ann. Chim. Phys.* **1903**, *28*, 433–530.
- (13) Sano, H.; Tachiya, M. Partially Diffusion-Controlled Recombination. *J. Chem. Phys.* **1979**, *71*, 1276–1282.
- (14) Sandanayaka, A. S. D.; Matsushima, T.; Bencheikh, F.; Yoshida, K.; Inoue, M.; Fujihara, T.; Goushi, K.; Ribierre, J. C.; Adachi, C. Toward Continuous-Wave Operation of Organic Semiconductor Lasers. *Science Advances*. **2017**, *3*, 1602570.
- (15) Zhao, J.; Yan, Y.; Gao, Z.; Du, Y.; Dong, H.; Yao, J.; Zhao, Y. Full-Color Laser Displays Based on Organic Printed Microlaser Arrays. *Nat. Commun.* **2019**, *10*, 870.
- (16) Wang, L.; Nan, G.; Yang, X.; Peng, Q.; Li, Q.; Shuai, Z. Computational Methods for Design of Organic Materials with High Charge Mobility. *Chem. Soc. Rev.* **2010**, *39*, 423–434.
- (17) Geng, H.; Peng, Q.; Wang, L.; Li, H.; Liao, Y.; Ma, Z.; Shuai, Z. Toward Quantitative Prediction of Charge Mobility in Organic Semiconductors: Tunneling Enabled Hopping Model. *Adv. Mater.* **2012**, *24*, 3568–3572.
- (18) Giri, G.; Verploegen, E.; Mannsfeld, S. C. B.; Atahan-Evrenk, S.; Kim, D. H.; Lee, S. Y.; Becerril, H. A.; Aspuru-Guzik, A.; Toney, M. F.; Bao, Z. Tuning Charge Transport in Solution-Sheared Organic Semiconductors Using Lattice Strain. *Nature* **2011**, *480*, 504–508.
- (19) Birks, J. B. *Photophysics of aromatic molecules*; Wiley-Interscience: London, UK, 1970.
- (20) Sundar, V. C.; Zaumseil, J.; Podzorov, V.; Menard, E.; Willett, R. L.; Someya, T.; Gershenson, M. E.; Rogers, J. A. Elastomeric Transistor Stamps: Reversible Probing of Charge Transport in Organic Crystals. *Science* **2004**, *303*, 1644–1646.
- (21) Wen, S. H.; Li, A.; Song, J.; Deng, W. Q.; Han, K. L.; Goddard, W. A. First-Principles Investigation of Anisotropic Hole Mobilities in Organic Semiconductors. *J. Phys. Chem. B* **2009**, *113*, 8813–8819.
- (22) Gao, F.; Liang, W.; Zhao, Y. Theoretical Studies of Vibrationally Resolved Absorption and Emission Spectra: from A Single Chromophore to Multichromophoric Oligomers/Aggregates. *Sci. China: Chem.* **2010**, *53*, 297–309.
- (23) Takeya, J.; Yamagishi, M.; Tominari, Y.; Hirahara, R.; Nakazawa, Y.; Nishikawa, T.; Kawase, T.; Shimoda, T.; Ogawa, S. Very High-Mobility Organic Single-Crystal Transistors with In-Crystal Conduction Channels. *Appl. Phys. Lett.* **2007**, *90*, 102120.
- (24) Takenobu, T.; Bisri, S. Z.; Takahashi, T.; Yahiro, M.; Adachi, C.; Iwasa, Y. High Current Density in Light-Emitting Transistors of Organic Single Crystals. *Phys. Rev. Lett.* **2008**, *100*, 066601.
- (25) Izawa, T.; Miyazaki, E.; Takimiya, K. Molecular Ordering of High-Performance Soluble Molecular Semiconductors and Re-Evaluation of Their Field-Effect Transistor Characteristics. *Adv. Mater.* **2008**, *20*, 3388–3392.
- (26) Yang, X.; Wang, L.; Wang, C.; Long, W.; Shuai, Z. Influences of Crystal Structures and Molecular Sizes on The Charge Mobility of Organic Semiconductors: Oligothiophenes. *Chem. Mater.* **2008**, *20*, 3205–3211.
- (27) Hajlaoui, R.; Horowitz, G.; Garnier, F.; Arcebrouchet, A.; Laigre, L.; Elkassmi, A.; Demanze, F.; Kouki, F. Improved Field-Effect Mobility in Short Oligothiophenes: Quaterthiophene and Quinquethiophene. *Adv. Mater.* **1997**, *9*, 389–391.
- (28) Ieujji, R.; Goushi, K.; Adachi, C. Triplet-Triplet Upconversion Enhanced By Spin-Orbit Coupling in Organic Light-Emitting Diodes. *Nat. Commun.* **2019**, *10*, 5283.

- (29) Huh, J. S.; Ha, Y. H.; Kwon, S. K.; Kim, Y. H.; Kim, J. J. Design Strategy of Anthracene-Based Fluorophores toward High-Efficiency Deep Blue Organic Light-Emitting Diodes Utilizing Triplet-Triplet Fusion. *ACS Appl. Mater. Interfaces* **2020**, *12*, 15422–15429.
- (30) Zambianchi, M.; Benvenuti, E.; Bettini, C.; Zanardi, C.; Seiber, R.; Gentili, D.; Cavallini, M.; Muccini, M.; Biondo, V.; Soldano, C.; et al. Anthracene-Based Molecular Emitters for Non-Doped Deep-Blue Organic Light Emitting Transistors. *J. Mater. Chem. C* **2016**, *4*, 9411–9417.
- (31) Zhang, Y.; Ye, J.; Liu, Z.; Liu, Q.; Guo, X.; Dang, Y.; Zhang, J.; Wei, Z.; Wang, Z.; Wang, Z.; et al. Red-Emissive Poly(Phenylene Vinylene)-Derived Semiconductors with Well-Balanced Ambipolar Electrical Transporting Properties. *J. Mater. Chem. C* **2020**, *8*, 10868–10879.
- (32) Meng, H.; Sun, F. P.; Goldfinger, M. B.; Jaycox, G. D.; Li, Z. G.; Marshall, W. J.; Blackman, G. S. High-Performance, Stable Organic Thin-Film Field-Effect Transistors Based on Bis-5'-Alkylthiophen-2'-yl-2,6-Anthracene Semiconductors. *J. Am. Chem. Soc.* **2005**, *127*, 2406–2407.
- (33) Jiang, L.; Hu, W.; Wei, Z.; Xu, W.; Meng, H. High-Performance Organic Single-Crystal Transistors and Digital Inverters of An Anthracene Derivative. *Adv. Mater.* **2009**, *21*, 3649–3653.
- (34) Yan, L.; Zhao, Y.; Yu, H.; Hu, Z.; He, Y.; Li, A.; Goto, O.; Yan, C.; Chen, T.; Chen, R.; et al. Influence of Heteroatoms on The Charge Mobility of Anthracene Derivatives. *J. Mater. Chem. C* **2016**, *4*, 3517–3522.
- (35) Chen, M.; Zhao, Y.; Yan, L.; Yang, S.; Zhu, Y.; Murtaza, I.; He, G.; Meng, H.; Huang, W. A Unique Blend of 2-Fluorenyl-2-Anthracene and 2-Anthryl-2-Anthracene Showing White Emission and High Charge Mobility. *Angew. Chem., Int. Ed.* **2017**, *56*, 722–727.
- (36) Liu, J.; Zhang, H.; Dong, H.; Meng, L.; Jiang, L.; Jiang, L.; Wang, Y.; Yu, J.; Sun, Y.; Hu, W.; et al. High Mobility Emissive Organic Semiconductor. *Nat. Commun.* **2015**, *6*, 10032.
- (37) Li, J.; Zhou, K.; Liu, J.; Zhen, Y.; Liu, L.; Zhang, J.; Dong, H.; Zhang, X.; Jiang, L.; Hu, W. Aromatic Extension at 2,6-Positions of Anthracene toward An Elegant Strategy for Organic Semiconductors with Efficient Charge Transport and Strong Solid State Emission. *J. Am. Chem. Soc.* **2017**, *139*, 17261–17264.
- (38) Hepp, A.; Heil, H.; Weise, W.; Ahles, M.; Schmechel, R.; von Seggern, H. Light-Emitting Field-Effect Transistor Based on A Tetracene Thin Film. *Phys. Rev. Lett.* **2003**, *91*, 157406.
- (39) Liu, Z.; Zhang, G.; Zhang, D. Molecular Materials That Can Both Emit Light and Conduct Charges: Strategies and Perspectives. *Chem. - Eur. J.* **2016**, *22*, 462–471.
- (40) Qin, Z.; Gao, H.; Liu, J.; Zhou, K.; Li, J.; Dang, Y.; Huang, L.; Deng, H.; Zhang, X.; Dong, H.; et al. High-Efficiency Single-Component Organic Light-Emitting Transistors. *Adv. Mater.* **2019**, *31*, 1903175.
- (41) Hochstrasser, R. M.; Kasha, M. Application of The Exciton Model to Monomolecular Lamellar Sys-Tems. *Photochem. Photochem. Photobiol.* **1964**, *3*, 317–331.
- (42) Clark, J.; Silva, C.; Friend, R. H.; Spano, F. C. Role of Intermolecular Coupling in The Photophysics of Disordered Organic Semiconductors: Aggregate Emission in Regioregular Polythiophene. *Phys. Rev. Lett.* **2007**, *98*, 206406.
- (43) Kasha, M. Energy Transfer Mechanisms and The Molecular Exciton Model for Molecular Aggregates. *Radiat. Res.* **2012**, *178*, AV27–AV34.
- (44) An, B. K.; Gierschner, J.; Park, S. Y.  $\pi$ -Conjugated Cyanostilbene Derivatives: A Unique Self-Assembly Motif for Molecular Nanostructures with Enhanced Emission and Transport. *Acc. Chem. Res.* **2012**, *45*, 544–554.
- (45) Cornil, J.; Beljonne, D.; Calbert, J. P.; Bredas, J. L. Interchain Interactions in Organic  $\pi$ -Conjugated Materials: Impact on Electronic Structure, Optical Response, and Charge Transport. *Adv. Mater.* **2001**, *13*, 1053–1067.
- (46) Hestand, N. J.; Spano, F. C. Molecular Aggregate Photophysics Beyond The Kasha Model: Novel Design Principles for Organic Materials. *Acc. Chem. Res.* **2017**, *50*, 341–350.
- (47) Mikhnenko, O. V.; Blom, P. W. M.; Nguyen, T. Q. Exciton Diffusion in Organic Semiconductors. *Energy Environ. Sci.* **2015**, *8*, 1867–1888.
- (48) Spano, F. C. Excitons in Conjugated Oligomer Aggregates, Films, and Crystals. *Annu. Rev. Phys. Chem.* **2006**, *57*, 217–243.
- (49) Mei, J.; Leung, N. L. C.; Kwok, R. T.; Lam, J. W.; Tang, B. Z. Aggregation-Induced Emission: Together We Shine, United We Soar. *Chem. Rev.* **2015**, *115*, 11718–11940.
- (50) Xie, Z.; Yang, B.; Li, F.; Cheng, G.; Liu, L.; Yang, G.; Xu, H.; Ye, L.; Hanif, M.; Liu, S.; et al. Cross Dipole Stacking in The Crystal of Distyrylbenzene Derivative: The Approach toward High Solid-State Luminescence Efficiency. *J. Am. Chem. Soc.* **2005**, *127*, 14152–14153.
- (51) Zhou, J.; Zhang, W.; Jiang, X.; Wang, C.; Zhou, X.; Xu, B.; Liu, L.; Xie, Z.; Ma, Y. Magic-Angle Stacking and Strong Intermolecular  $\pi$ - $\pi$  Interaction in A Perylene Bisimide Crystal: An Approach for Efficient Near-infrared (NIR) Emission and High Electron Mobility. *J. Phys. Chem. Lett.* **2018**, *9*, 596–600.
- (52) Singh, N. J.; Min, S. K.; Kim, D. Y.; Kim, K. S. Comprehensive Energy Analysis for Various Types of  $\pi$ -Interaction. *J. Chem. Theory Comput.* **2009**, *5*, 515–529.
- (53) Sherrill, C. D. Energy Component Analysis of  $\pi$  Interactions. *Acc. Chem. Res.* **2013**, *46*, 1020–1028.
- (54) Shuai, Z.; Geng, H.; Xu, W.; Liao, Y.; Andre, J. M. From Charge Transport Parameters to Charge Mobility in Organic Semiconductors Through Multiscale Simulation. *Chem. Soc. Rev.* **2014**, *43*, 2662–2679.
- (55) Li, W.; Peng, Q.; Xie, Y.; Zhang, T.; Shuai, Z. Effect of Intermolecular Excited-State Interaction on Vibrationally Resolved Optical Spectra in Organic Molecular Aggregates. *Huaxue Xuebao* **2016**, *74*, 902.
- (56) Li, W.; Zhu, L.; Shi, Q.; Ren, J.; Peng, Q.; Shuai, Z. Excitonic Coupling Effect on The Nonradiative Decay Rate in Molecular Aggregates: Formalism and Application. *Chem. Phys. Lett.* **2017**, *683*, 507–514.
- (57) Li, W.; Peng, Q.; Ma, H.; Wen, J.; Ma, J.; Peteanu, L. A.; Shuai, Z. Theoretical Investigations on The Roles of Intramolecular Structure Distortion Versus Irregular Intermolecular Packing in Optical Spectra of 6T Nanoparticles. *Chem. Mater.* **2017**, *29*, 2513–2520.
- (58) Carter-Fenk, K.; Lao, K. U.; Liu, K. Y.; Herbert, J. M. Accurate and Efficient Ab Initio Calculations for Supramolecular Complexes: Symmetry-Adapted Perturbation Theory with Many-Body Dispersion. *J. Phys. Chem. Lett.* **2019**, *10*, 2706–2714.
- (59) Shao, Y.; Gan, Z.; Epifanovsky, E.; Gilbert, A. T. B.; Wormit, M.; Kussmann, J.; Lange, A. W.; Behn, A.; Deng, J.; Feng, X.; et al. Advances in Molecular Quantum Chemistry Contained in The Q-Chem 4 Program Package. *Mol. Phys.* **2015**, *113*, 184–215.
- (60) Ostrowski, D. P.; Lytwak, L. A.; Mejia, M. L.; Stevenson, K. J.; Holliday, B. J.; Vanden Bout, D. A. The Effects of Aggregation on Electronic and Optical Properties of Oligothiophene Particles. *ACS Nano* **2012**, *6*, 5507–5513.
- (61) Blülle, B.; Troisi, A.; Häusermann, R.; Batlogg, B. Charge Transport Perpendicular to The High Mobility Plane in Organic Crystals: Bandlike Temperature Dependence Maintained Despite Hundredfold Anisotropy. *Phys. Rev. B: Condens. Matter Mater. Phys.* **2016**, *93*, 035205.
- (62) Scholes, G. D. Long-Range Resonance Energy Transfer in Molecular Systems. *Annu. Rev. Phys. Chem.* **2003**, *54*, 57–87.
- (63) Sanchez-Carrera, R. S.; Atahan, S.; Schrier, J.; Aspuru-Guzik, A. Theoretical Characterization of The Air-Stable, High-Mobility Dinaphtho [2,3-b:2'3'-f]Thieno[3,2-b]-Thiophene Organic Semiconductor. *J. Phys. Chem. C* **2010**, *114*, 2334–2340.
- (64) Shi, W.; Chen, J.; Xi, J.; Wang, D.; Shuai, Z. Search for Organic Thermoelectric Materials with High Mobility: The Case of 2,7-Dialkyl[1]Benzothieno[3,2-b][1]Benzothiophene Derivatives. *Chem. Mater.* **2014**, *26*, 2669–2677.
- (65) Coropceanu, V.; Cornil, J.; da Silva Filho, D. A.; Olivier, Y.; Silbey, R.; Bredas, J. L. Charge Transport in Organic Semiconductors. *Chem. Rev.* **2007**, *107*, 2165–2165.

(66) Troisi, A.; Orlandi, G. Band Structure of The Four Pentacene Polymorphs and Effect on The Hole Mobility at Low Temperature. *J. Phys. Chem. B* **2005**, *109*, 1849–1856.

(67) Hestand, N. J.; Spano, F. C. Molecular Aggregate Photophysics Beyond The Kasha Model: Novel Design Principles for Organic Materials. *Acc. Chem. Res.* **2017**, *50*, 341–350.

(68) Song, J.; Gao, F.; Shi, B.; Liang, W. Identification of The Mechanism of Enhanced Exciton Interaction in Rigidly Linked Naphthalene Dimers. *Phys. Chem. Chem. Phys.* **2010**, *12*, 13070–13075.

#### ■ NOTE ADDED AFTER ASAP PUBLICATION

Due to an ACS production error, this paper was originally published ASAP with incorrect pagination. This was corrected in the version published on January 14, 2021.